

Steady-state traffic flow on a ring road with up- and down- slopes

Chun-Xiu Wu^{1,3} Peng Zhang^{1,3*} S.C. Wong² Keechoo Choi⁴

1. Shanghai Institute of Applied Mathematics and Mechanics, Shanghai University,
Shanghai, P.R. China

2. Department of Civil Engineering, The University of Hong Kong, Pokfulam Road,
Hong Kong SAR, P.R. China

3. Shanghai Key Laboratory of Mechanics in Energy Engineering

4 Department of Transportation Engineering, TOD-based Sustainable Urban Transportation Center,
Ajou University, Korea

Abstract: This paper studies steady-state traffic flow on a ring road with up- and down- slopes using a semi-discrete model. By exploiting the relations between the semi-discrete and the continuum models, a steady-state solution is uniquely determined for a given total number of vehicles on the ring road. The solution is exact and always stable with respect to the first-order continuum model, whereas it is a good approximation with respect to the semi-discrete model provided that the involved equilibrium constant states are linearly stable. In an otherwise case, the instability of one or more equilibria could trigger stop-and-go waves propagating in certain road sections or throughout the ring road. The indicated results are reasonable and thus physically significant for a better understanding of real traffic flow on an inhomogeneous road.

Keywords: semi-discrete model; inhomogeneous road conditions; discontinuous fluxes; bottleneck; instability

1 Introduction

Traffic flow problem with inhomogeneous road conditions has been studied by using the macroscopic continuum model and the microscopic car-following model. In the former formulation, the Riemann problem was concerned mainly for designing a numerical scheme, which could be related to the

*Corresponding author. E-mail: pzhang@mail.shu.edu.cn.

theory of hyperbolic conservation laws with discontinuous fluxes [1–8]. In the latter formulation, steady-state flow was analytically or numerically studied by assuming or implying that the solution is piecewise equilibrium constant in the inhomogeneous road sections [9–14].

Actually, such a steady-state solution could be described by using the theory of hyperbolic conservation laws with discontinuous fluxes [5, 12], which is exact and stable for the first-order continuum LWR model [15, 16]. However, it is only an approximate solution to the car-following model or the higher-order model with relaxation if the relaxation time is sufficiently small; otherwise, it is unnecessarily stable due to the underlying metastability in these models. Nevertheless, this feature has not yet been well realized or emphasized in the aforementioned studies of the car-following model.

In the context, the present paper discusses the problem by using a semi-discrete model, which can be viewed as an extension of and thus is more general than the car-following model [17]. On the one hand, we enhance the mathematical analysis of steady-state flow on a ring road with up- and down- slopes, which poses more complexity for the solution. On the other hand, the instability of the solution is emphasized with physical interpretation through analysis of all equilibrium states as well as numerical simulation. Actually, equilibrium traffic flow with an intermediate density value is widely regarded as unstable on a homogeneous ring road, which with oscillations is liable to evolve into stop-and-go waves (e.g., see [18–21]). Although the discussed ring road is much more complicated, and the simulation does not completely agree with the analytical results due to errors in the analysis, the steady-state solution is indicated to have similar tendency. That is, it is highly stable for a large or small number of vehicles on the ring road; it is unstable for the case that is between. This result is significant for a better understanding of macroscopic properties of traffic flow on an inhomogeneous road. Although not directly applicable, the instabilities could be further associated with those typically indicated in [22–24] and those analytically studied in [25, 26].

The remainder of the paper is organized as follows. In Section 2, the semi-discrete model together with its correlation to the continuum model is discussed, and the linear stability condition for an equilibrium solution state is indicated. In Section 3, the wave pattern at a stationary interface is described by using the theory of hyperbolic conservation laws with discontinuous fluxes, which helps determine the two adjacent equilibrium constant states. Accordingly, the wave types of the steady-state solution on a ring road with up- and down- slopes are analytically indicated, which depend on the total number of vehicles on the ring road. In Section 4, initial distributions with certain total number of vehicles are shown to converge to or diverge from the corresponding steady-state solutions through numerical simulation, which agrees with the analytical results in general. We conclude the paper by Section 5.

2 The semi-discrete model

In the semi-discrete model [17], a moving “particle” in traffic flow could be numbered by m with $x_m(t)$ being its position, and

$$\frac{dx_m(t)}{dt} = u_m(t), \quad m = 0, \pm 1, \pm 2, \dots \quad (1)$$

being its speed, and the acceleration was defined through

$$\frac{d}{dt}[u_m(t) + p(s_m(t))] = \frac{1}{\tau}[u_e(s_m(t)) - u_m(t)]. \quad (2)$$

Here,

$$s_m(t) = [x_{m+1}(t) - x_m(t)]/\Delta M, \quad \text{and } \rho_m(t) \equiv (s_m(t))^{-1}, \quad (3)$$

are the specific volume and the density represented by the particle m , ΔM is the mass between the particles m and $m+1$, $u_e(s)$ and $p(s)$ are the equilibrium velocity-density relationship and the traffic pressure satisfying $u'_e(s) > 0$, and $p'(s) \leq 0$. For $\Delta M = 1$, the semi-discrete model of (1) and (2) reduces to a car-following model, in which case each particle can be viewed as a vehicle in that there is just one vehicle between the heads of two adjacent vehicles. The resultant car-following model is essentially the same as that in [27–29].

2.1 The correlation to the continuum model in Lagrange coordinates

Assume that there is no overtake between particles for division with a sufficiently small increment ΔM , and let M denote the total mass not passing through the particle m . This implies that M referring to the particle m is independent of time t . Therefore, the particle m can be identified by M and an associated variable $A_m(t)$ (e.g., the position $x_m(t)$ and speed $v_m(t)$) can be re-denoted by $A(M, t)$. Let $\Delta M \rightarrow 0$, then the flow can be viewed as a continuum, in which M and t constitute the Lagrange coordinate system to describe the variable $A(M, t)$. In this case, Eq. (3) gives

$$s(M, t) = x_M(M, t), \quad \text{and } \rho(M, t) = (s(M, t))^{-1}. \quad (4)$$

Furthermore, we reduce Eq. (1) from $dx_{m+1}(t)/dt = u_{m+1}(t)$, and divide the resultant equation by ΔM . Then, for $\Delta M \rightarrow 0$, we have the following partially differential equation:

$$s_t(M, t) - u_M(M, t) = 0. \quad (5)$$

It is obvious that, for $\Delta M \rightarrow 0$, Eq. (2) yields

$$[u(M, t) + p(s(M, t))]_t = \frac{u_e(s(M, t)) - u(M, t)}{\tau}. \quad (6)$$

The discussion implies the consistency between the semi-discrete model (1)-(2) and the continuum model (5)-(6), namely, the former system converges to the latter system for $\Delta M \rightarrow 0$. See [17] for more detailed discussion of the Lagrange coordinates.

2.2 The correlation to the continuum model in Euler coordinates

Let now $A(M, t)$ be denoted by the Euler coordinates (x, t) with $A(M, t) = A(x, t)$, where $x = x(M, t)$ is the position. We have

$$A_t(x, t) = A_x(x, t)x_t(M, t) + A_t(x, t), \quad A_M(x, t) = A_x(x, t)x_M(M, t), \quad (7)$$

where $x_t(M, t) = u(M, t) = u(x, t)$, and $x_M(M, t) = s(M, t) = s(x, t) = 1/\rho(x, t)$, according to Eqs. (1) and (4). Replacing the partial derivatives of $s(M, t)$ and $u(M, t)$ in Eqs. (5)-(6) through Eq. (7), we have

$$\rho_t + (\rho u)_x = 0, \quad (8)$$

$$[\rho(u + P(\rho))]_t + [\rho u(u + P(\rho))]_x = \frac{\rho U_e(\rho) - \rho u}{\tau}, \quad (9)$$

where $P(\rho) = p(s)$, $U_e(\rho) = u_e(s)$, and $\rho = 1/s$. The system of (8)-(9) turns out to be the so called “anisotropic” higher-order traffic flow models in [30–33]. This again establishes the correlation between the microscopic semi-discrete model and the macroscopic continuum model.

The consistence between the aforementioned three systems implies that the solution to the semi-discrete model should converge to the solution to the other two systems for $\Delta M \rightarrow 0$.

2.3 Stability of equilibrium solution

An equilibrium constant state $(\rho_0, U_e(\rho_0))$ or $(s_0, u_e(s_0))$ is linearly stable with respect to the higher-order model (8)-(9) or (5)-(6), if

$$U'_e(\rho_0) + P'(\rho_0) \geq 0, \quad \text{or} \quad u'_e(s_0) + p'(s_0) \leq 0. \quad (10)$$

This corresponds to an equilibrium state

$$x_{m+1}^0(t) - x_m^0(t) = s_0 \Delta M, \quad \text{or} \quad x_m^0(t) = u_e(s_0)t + m \Delta M s_0, \quad (11)$$

in the semi-discrete model (1)-(2), which is linearly stable if

$$u'_e(s_0) + p'(s_0) \leq \frac{\Delta M}{2\tau}. \quad (12)$$

As $\Delta M \rightarrow 0$, Eq. (12) reduces to Eq. (10), which also indicates the consistency between the continuum and the semi-discrete models. See [17] for detailed discussion.

3 The steady-state solution over inhomogeneous road sections

For discussion of the steady-state solution, the system (8)-(9) under the Euler coordinates is convenient to deal with the interface between two inhomogeneous road sections. For sufficient small τ , Eq. (9) is approximated by $u = U_e(\rho)$, which together with Eq. (8) leads to the following LWR model [15, 16]:

$$\rho_t + (Q_e(\rho))_x = 0, \quad (13)$$

where $Q_e(\rho) = \rho U_e(\rho)$ is the flow-density relationship or fundamental diagram.

3.1 General discussion of the solution

In general, the steady-state solution $(\rho(x, t), u(x, t)) = (\rho(x), u(x))$ of (13) on an inhomogeneous road is piecewise constant satisfying the equilibrium condition $u(x) = U_e(\rho(x))$. At each dividing point or interface, the flow $q \equiv \rho u = Q_e(\rho)$ is continuous and thus is constant all over the road. However, the density $\rho(x)$ and the velocity $u(x)$ are usually discontinuous at the dividing point, which can be either a contact between two inhomogeneous road sections or a stationary shock in a homogeneous road section.

The constancy of the flow at the dividing point is attributed to the mass conservation or the Rankine-Hugoniot condition (see [2–5] and the references therein). Let $\rho = \rho_{\mp}$ and Q_e^{\mp} denote the densities and fundamental diagrams on the left and right hand sides of the interface. Then, the mass conservation is simply that

$$Q_e^-(\rho_-) = Q_e^+(\rho_+). \quad (14)$$

For the dividing point which is stationary, a “wave entropy” condition can be applied at the interface to describe valid wave breaking on the both sides [2–5]. That is, the characteristic speeds on the two sides take the same sign with

$$(Q_e^-(\rho_-))'(Q_e^+(\rho_+))' > 0. \quad (15)$$

Otherwise, we have

$$(Q_e^+(\rho_+))' \geq 0, \text{ if } (Q_e^-(\rho_-))' = 0; \quad (16)$$

and

$$(Q_e^-(\rho_-))' \leq 0, \text{ if } (Q_e^+(\rho_+))' = 0. \quad (17)$$

See also [6, 7] for a similar entropy condition.

We assume that the critical densities are ρ_-^* and ρ_+^* with $Q_e(\rho_-^*)$ and $Q_e(\rho_+^*)$ being the maximal flows or capacities on the left and the right hand sides, i.e.,

$$(Q_e^\mp(\rho_\pm^*))' = 0; (\rho - \rho_\pm^*)(Q_e^\mp(\rho))' < 0, \text{ for } \rho \neq \rho_\pm^*. \quad (18)$$

For the discussed steady-state solution $\rho = \rho(x)$, we obviously have

$$Q_e(\rho(x)) \leq \min(Q_e^-(\rho_-^*), Q_e^+(\rho_+^*)), \quad (19)$$

and the term on the right hand side is defined as the capacity with respect to the two divided sections. Thus, we have four wave patterns at the interface (Fig. 1). The normal and the congested wave patterns (Figs. 1(a) and (d)) are associated with Eq. (15). The upstream or downstream capacitated wave patterns (Fig. 1(b) or (c)) is associated with Eq. (16) or (17), which occurs only if $Q_e^-(\rho_-^*) \leq Q_e^+(\rho_+^*)$ or vice verse. We call the interface a bottleneck if $Q_e^-(\rho_-^*) > Q_e^+(\rho_+^*)$, which triggers a queue upstream from the interface when the traffic is downstream capacitated.

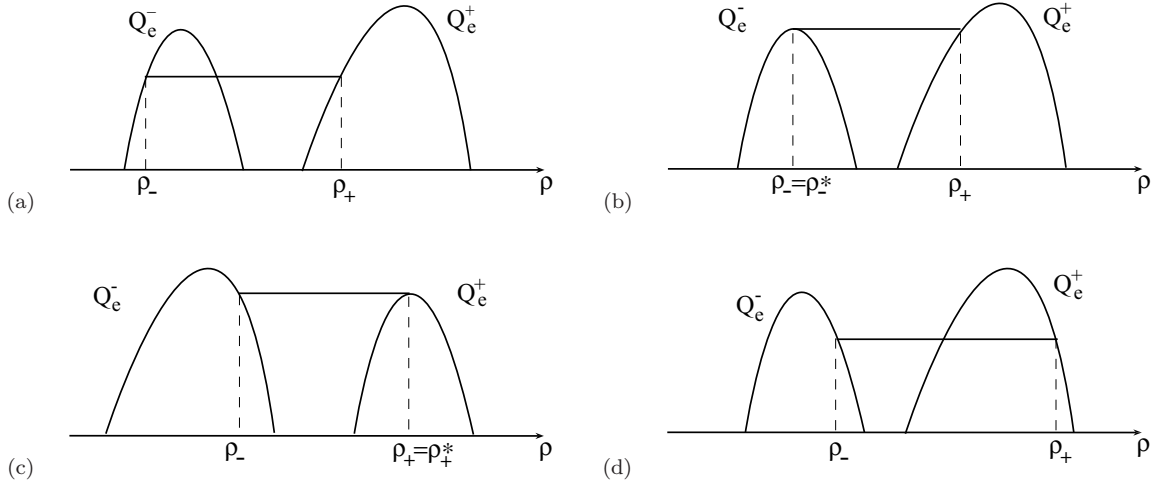


Fig. 1 Four wave patterns at a joint between two inhomogeneous road sections, which obeys the conservation of (11). (a) and (d): normal and congested wave patterns associated with Eq. (15); (b) and (c): upstream and downstream capacitated wave pattern associated with Eqs. (16) and (17), respectively.

3.2 The solution on a ring road with up- and down- slopes

Steady-state flow on an inhomogeneous highway road is characterized by the wave pattern at each of the interfaces. For a road with up- and down- slopes, we adopt the following velocity-specific volume relationship:

$$u_e(s) = \frac{u_f(\beta)[\tanh(s/l - x_c(\beta)/l) + \tanh(x_c(\beta)/l - 1)]}{1 + \tanh(x_c(\beta)/l - 1)}, \quad (20)$$

where β is the slope, l the vehicle length, and $u_f(\beta)$ the free flow velocity. We can easily examine that $u_e(l) = 0$, $u_e(+\infty) = u_f(\beta)$, and $u'_e(s) > 0$, for $s \geq l$. By the relations: $U_e(\rho) = u_e(s)$, $\rho = s^{-1}$, we correspondingly have $U'_e(\rho) < 0$, for $\rho \in [0, \rho_{jam}]$, and $U_e(\rho_{jam}) = 0$, $U_e(0) = u_f(\beta)$, where $\rho_{jam} = 1/l$ is the jamming density. By scaling, the free flow velocity $u_f(\beta)$ and the safe interval $x_c(\beta)$ are determined by the following piecewise functions:

$$\frac{u_f(\beta)}{u_f(0)} = \begin{cases} -100\beta^2 - 5\beta + 1, & -0.10 \leq \beta < 0, \\ 1, & 0 \leq \beta < 0.02, \\ -150\beta^2 + 3\beta + 1, & 0.02 \leq \beta \leq 0.08, \\ 0.28, & 0.08 < \beta \leq 0.10, \end{cases} \quad u_f(0) = 30 \text{ m/s}, \quad (21)$$

and

$$\frac{x_c(\beta)}{l} = \begin{cases} 300\beta^2 - 12\beta + 3, & -0.10 \leq \beta < 0, \\ 80\beta^2 + 15\beta + 3, & 0 \leq \beta \leq 0.10, \end{cases} \quad l = 4.5 \text{ m}, \quad (22)$$

The formula (20) is extended from that in [28], and Eqs. (21)-(22) are based on the experimental study in [34]. The formula (20) can also be viewed as a modification of that in [13], which was extended from that in [35]. We note that the properties of (18) can be verified for $|\beta| \leq 0.1$.

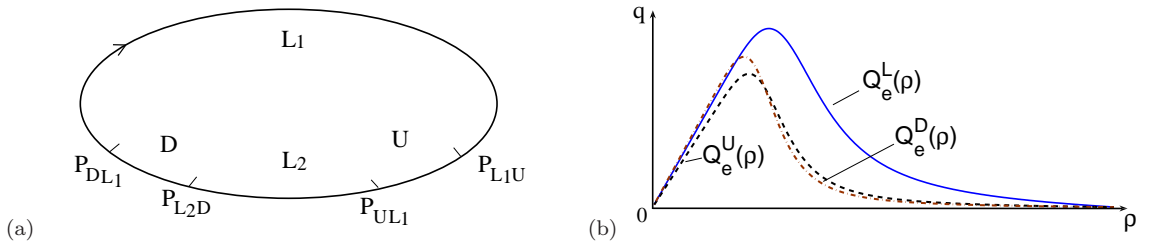


Fig. 2 (a) The clockwise ring road $R = L_1 \cup U \cup L_2 \cup D$, with the lengths $|R| = 6750\text{m}$, $|L_1| = 4050\text{m}$, $|U| = 675\text{m}$, and $|D| = 675\text{m}$; (b) the fundamental diagrams $q = Q_e^L(\rho)$, $q = Q_e^U(\rho)$, and $q = Q_e^D(\rho)$, for the level road sections $L_1 \cup L_2$, the up-slope section U , and the down-slope section D , which are defined through Eqs. (20)-(22).

We now consider a clockwise ring road R which is composed of four sections: (i) the level road L_1 with $\beta = 0$; the up-slope U with $\beta = 0.04$; the level road L_2 with $\beta = 0$; and the down-slope D with $\beta = -0.04$. The joints between two adjacent sections are denoted by P_{L_1U} , P_{UL_2} , P_{L_2D} , and P_{DL_1} . The ring road is shown in Fig. 2(a), and the fundamental diagrams $q = Q_e(\rho)$ for all sections are shown in Fig. 2(b). We see that, by Fig. 2(b),

$$Q_s \leq \min(Q_e^L(\rho_L^*), Q_e^U(\rho_U^*), Q_e^D(\rho_D^*)) = Q_e^U(\rho_U^*) \equiv Q_c, \quad (23)$$

where $Q_s = Q_e(\rho(x))$ is the flow corresponding to the steady-state solution $\rho(x)$, and Q_c is defined as the capacity of the ring road. Eq. (23) is the extension of Eq. (19). Given Q_s , we have two solution

values of $\rho(x)$ through Eqs. (20)-(22). However, $\rho(x)$ can be uniquely determined according to the wave pattern at each dividing point. Actually, Q_s together with the wave patterns can be uniquely determined by the total number N of vehicles on the ring road, which is indicated in the following discussion by referring to Figs. 2(a) and (b).

For N increasing from $N = 0$, Q_s increases until it reaches the capacity with $Q_s = Q_c$, when the total number of vehicles

$$N_{t_1} = \sum_{\chi} |\chi| \rho_{\chi}, \quad \chi = L_1, U, L_2, D. \quad (24)$$

Here, $|\chi|$ and ρ_{χ} represent the lengths of and the densities in four sections divided by P_{L_1U} , P_{UL_2} , P_{L_2D} , and P_{DL_1} . In this case, we have $\rho_{\chi} < \rho_{\chi}^*$, except for $\rho_U = \rho_U^*$.

For $N < N_{t_1}$, we have $Q_s < Q_c$, and $\rho_{\chi} < \rho_{\chi}^*$, for all χ , thus the interfaces at all dividing points represent normal wave patterns, which are associated with Eqs. (11)-(12). Accordingly, the constant flow Q_s together with the densities ρ_{χ} in the four sections is uniquely determined by

$$\sum_{\chi} |\chi| \rho_{\chi} = N, \quad Q_e(\rho_{\chi}) = Q_s, \quad \chi = L_1, U, L_2, D. \quad (25)$$

For $N > N_{t_1}$, we have the same flow rate $Q_s = Q_c$, and other density values as those in the case of $N = N_{t_1}$, except for a “blow-up” upstream from P_{L_1U} , which is due to the capacity drop $Q_e(\rho_U^*) = Q_c < Q_e(\rho_L^*)$ (see Eq. (23) and Fig. 2(b)) at this interface. According to the discussion in Section 3.1, this suggests that P_{L_1U} represent the one and only bottleneck on the whole road with respect to the discussed solution. In this case, L_1 is divided into two intervals L_{11} and L_{12} , and their lengths together with the dividing point are determined by N through the following equation:

$$N = \sum_{\chi} |\chi| \rho_{\chi}, \quad \chi = L_{11}, L_{12}, U, L_2, D. \quad (26)$$

In this case, the traffic is downstream capacitated at P_{L_1U} , and $P_{L_{11}L_{12}}$ represents the position P_s of a stationary shock; the threshold value of N is computed by

$$N_{t_2} = \sum_{\chi} |\chi| \rho_{\chi}, \quad \chi = L_1, U, L_2, D, \quad (27)$$

when P_s coincides with P_{DL_1} .

As N continues to increase, the position P_s of the stationary shock moves upstream until it reaches the joint P_{UL_2} , which is between the up-slope and the level road 2. In this process, a joint becomes to represent a congested wave pattern if its position is downstream from P_s . We have the threshold value

$$N_{t_3} = \sum_{\chi} |\chi| \rho_{\chi}, \quad \chi = L_1, U, L_2, D, \quad (28)$$

when P_s coincides with P_{L_2D} , and the threshold value

$$N_{t_4} = \sum_{\chi} |\chi| \rho_{\chi}, \quad \chi = L_1, U, L_2, D, \quad (29)$$

when P_s coincides with P_{UL_2} . The solution $\rho(x)$ together with the position P_s of the stationary shock for N between N_{t_i} and $N_{t_{i+1}}$ ($i = 2, 3$) can be determined similarly to Eq. (26).

For $N > N_{t_4}$, the constant flow Q_s cannot reach the capacity Q_c of the ring road. As N increases, Q_s begins to decrease until $Q_s = 0$, when the whole road becomes completely blocked. In this development, Q_s together with ρ_{χ} in the four sections is determined also by Eq. (25), except that each joint between two adjacent road sections represents a congested wave pattern.

The function $Q_s = Q_s(N)$ is shown in Fig. 3(a). Correspondingly, the characteristics of the wave patterns at all joints are shown in Fig. 3(b).

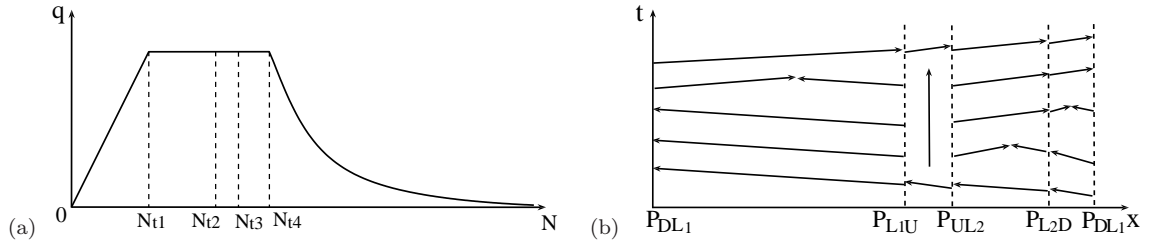


Fig. 3 (a) The function $Q_s = Q_s(N)$; (b) resultant wave patterns at all joints for $N < N_{t_1}$, $N_{t_1} < N < N_{t_2}$, $N_{t_2} < N < N_{t_3}$, $N_{t_3} < N < N_{t_4}$, and $N > N_{t_4}$, from the top to the bottom, respectively, where the left, up and right arrows represent negative, zero and positive characteristic speeds, respectively, and a position intersected by a left arrow and a right arrow represents a stationary shock.

4 Numerical simulation

The semi-discrete model of (1)-(2) is used for numerical simulation. We casually set the following initial distribution:

$$s_0 = \frac{|R|}{N}, \quad x_m(0) = ms_0, \quad v_m(0) = u_e(s_0), \quad m = 1, \dots, N, \quad (30)$$

and define $s_N(t) = (x_1(t) + |R| - x_N(t))/\Delta M$ in Eq. (2), where the length of the ring road $|R| = 6750m$. In the simulation, the position that is 2700 meters downstream from the joint P_{L_1U} is taken as the origin. Moreover, the length of a road section is scaled by $l = 4.5m$ and the density is scaled by $\rho_{jam} = 1/l$. As a consequence, the coordinates of the joints P_{L_1U} , P_{UL_2} , P_{L_2D} , and P_{DL_1} are 600, 750, 1050, and 1200, respectively.

Since $u_e(s_0)$ in Eq. (30) depends on the slope β , the vehicular velocities in different road sections are not equal. As a consequence, the headway cannot keep constant in the evolution. Then, given

the total number N of vehicles on the ring road, the simulation is designed to test whether the initial distribution of (30) converges to the corresponding steady-state solution. Since the simulation involves a stiff relaxation with small τ , a semi-implicit scheme for time discretization of (1)-(2) is adopted,

$$\frac{x_m^{(n+1)} - x_m^{(n)}}{\Delta t} = u_m^{(n)}, \quad \frac{u_m^{(n+1)} + p(s_m^{(n+1)}) - u_m^{(n)} - p(s_m^{(n)})}{\Delta t} = \frac{u_e(s_m^{(n)}) - u_m^{(n+1)}}{\tau}, \quad (31)$$

where $s_m^{(n)} = x_{m+1}^{(n)} - x_m^{(n)}$.

The convergence or divergence is actually associated with the stability or instability of the discussed steady-state solution, for which the linear stability condition of (12) for the involved equilibrium states are referred to for comparison. However, we should note that not all lengths of these equilibrium states are adequate to apply Eq. (12), and that the coupling effect between two adjacent equilibrium states is neglected. Moreover, the perturbation arising from (30) to the corresponding steady-state solution can be hardly regarded as “small”. These should give rise to considerable errors in the comparison.

Table 1 Comparison between equilibrium values of the steady-state solution and simulated mean values of the semi-discrete model on the divided sections. The initial distribution of (30) always converges to the steady-state solution for sufficiently small relaxation time ($\tau = 0.03s$); it may diverge from the steady-state solution for large relaxation time ($\tau = 0.3s$), which brings about unstable equilibrium states of the solution.

N	analytical equilibrium values				simulated with $\tau = 0.03s$				simulated with $\tau = 0.3s$			
	L_1	U	L_2	D	L_1	U	L_2	D	L_1	U	L_2	D
250	.1610	.2228	.1610	.1557	.1633	.2000	.1633	.1600	.1633	.2000	.1633	.1600
330	.1644	.2080	.1644	.1592	.1648	.2133	.1633	.1600	.1670	.2000	.1633	.1600
	.3329				.3326				.3348			
420	.3329	.2080	.1644	.2297	.3322	.2067	.1667	.2333	.3333	.2000	.1778	.2133
			.3329				.3333				.3333	
550	.3906	.2749	.3906	.2667	.3911	.2733	.3900	.2667	.4111	.2667	.3433	.2467
620	.4418	.3061	.4418	.2930	.4400	.3067	.4433	.3000	.5089	.2133	.3267	.2133
675	.4824	.3285	.4824	.3124	.4833	.3267	.4767	.3200	.4833	.3267	.4800	.3133

We choose $\Delta M = 1$ to implement a realistic car-following simulation, in which case the particle m represents a vehicle and $s_m(t)$ is headway between the vehicles m and $m + 1$. Even ΔM is not so small, we show the convergence for τ that is sufficiently small to ensure the stability condition of (12) for all s_0 . Table 1 shows sets of simulated mean density values for comparison with the equilibrium density values of the corresponding steady-state solution that is discussed in Section 3.1. The simulated results are also shown in Fig. 4, by which we clearly observe the convergence.

In this case, the semi-discrete model together with its full discrete form of (31) works similarly to a relaxation scheme for solving the LWR model of (13) (see [36–38] for detailed discussion of the relaxation scheme).

However, it is more physically significant to deal with unstable traffic flow in the ring road by taking a much larger relaxation time, by which Eq. (12) suggests a narrower region of s_0 for the stability of the involved equilibrium states. We take $\tau = 0.3s$, which is more realistic when compared with those that are widely used for the car-following model in the literature. With the same values of N , the simulated mean values are also given in Table 1, and the simulation results are also shown in Fig. 4 to observe the convergence or divergence.

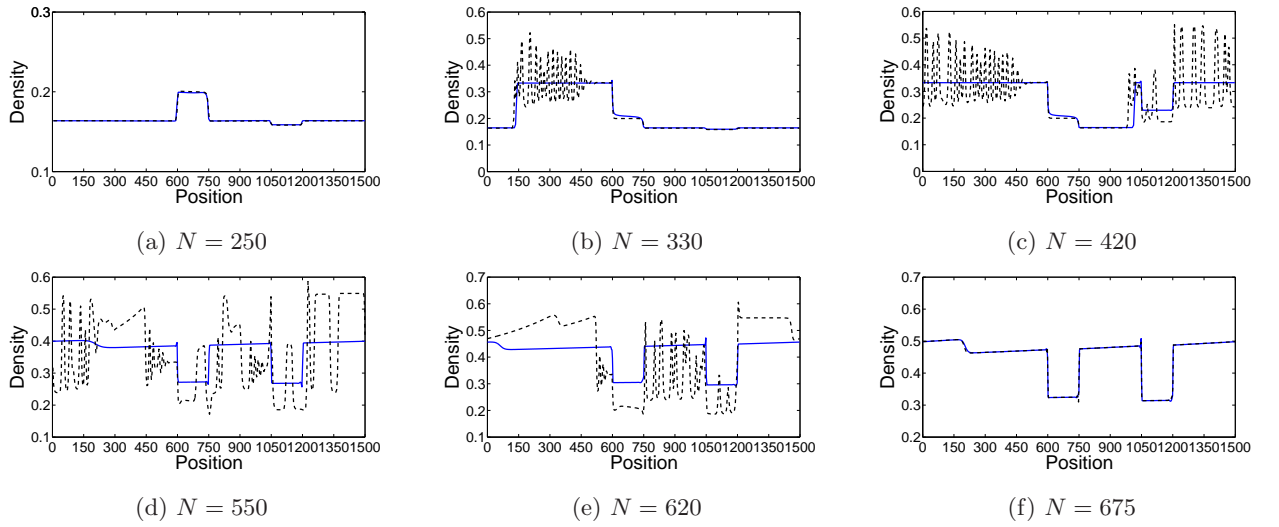


Fig. 4 Evolution of traffic flow on the ring road with initial distribution of (30) and for a long simulation time T . The density distributions at $T = 1500s$, for $\tau = 0.03s$ (blue and real line) and $\tau = 0.3s$ (black and dotted line). The coordinates of the joints P_{L_1U} , P_{UL_2} , P_{L_2D} , and P_{DL_1} are 600, 750, 1050, and 1200, respectively

All involved equilibrium states as well as their stability (for $\tau = 0.3s$) depend on the total number N of vehicles in the ring road, which is again taken as a characteristic parameter, and of which the threshold values for changes in stability are combined with those in Eqs. (24) and (27)-(29) to further classify the solution (see also Fig. 3). Table 2 indicates the solution properties especially the stability (S) or instability (I) of the equilibrium states with respect to the semi-discrete model, which is according to Eq. (12).

Table 2 agrees with Fig. 4 except for some inconsistency in the stability of the equilibrium states of the semi-discrete model, which corresponds to Fig. 4(e). However, both Table 2 and Fig. 4 indicate a similar tendency. That is, the whole solution is quite stable and convergent to the steady-state solution for small or large N ; the occurrence of instability becomes frequent and intensive for

N that is between. This tendency is similar to (but is more complex than) that for a homogeneous level ring road, which was indicated by both theoretical and experimental studies [18–21, 39].

Table 2 Changes in solution properties arising from changes in N . The second column shows the monotone change of $Q_s = Q_s(N)$, where the threshold values $N_{t_1} = 253$, $N_{t_2} = 404$, $N_{t_3} = 415$, and $N_{t_4} = 466$ are determined by Eqs. (21) and (23)-(26) (also compare with Fig. 3). Other columns show the stability (S) or instability (I) of the involved equilibrium states by using Eq. (29) with $\tau = 0.3s$.

N	Q_s	L_1	U	L_2	D
$[0, 253]$	\nearrow	S	S	S	S
$(253, 404)$	$= Q_c$	(S, I)	S	S	S
$[404, 415)$	$= Q_c$	I	S	S	(S, I)
$[415, 466)$	$= Q_c$	I	S	(S, I)	I
$[466, 478]$	\searrow	I	S	I	I
$(478, 579)$	\searrow	I	I	I	I
$[579, 637)$	\searrow	S	I	S	I
$[637, 657)$	\searrow	S	S	S	I
$[657, 1500]$	\searrow	S	S	S	S

Most oscillations in Figs. 4(b)-(e) represent stop and go waves in traffic. Among these, the waves in Figs. 4(b)-(c) demonstrate propagations only within one or more road sections, while we observe steady-state traffic flow in other road sections through comparison with the simulated results for $\tau = 0.03s$. In contrast, the waves in Figs. (d)-(e) propagate throughout the ring-road, in which case no steady states are locally observed. On the other hand, we see some regularity of the backward moving stop-and-go waves, which are somewhat similar to (but not as regular as) those traveling waves that were studied under homogeneous ring road conditions [17–20, 28]. The described solution properties change little for much longer simulations. Fig. 5 shows the evolution process for $N = 550$, which corresponds to Fig. 4(d).

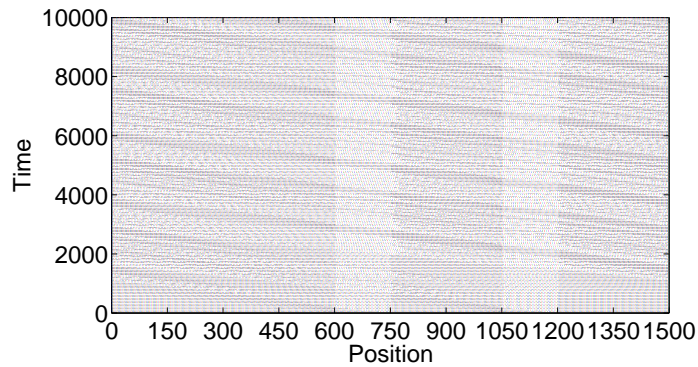


Fig. 5 Evolution of the initial distribution of (30) with $N = 550$ and for $t \leq 1500s$, which indicates stop-and-go waves moving backward throughout the ring-road.

5 Conclusions

We thoroughly investigate the steady-state solution on an inhomogeneous ring road using a semi-discrete model. According to the analysis of the wave pattern at a dividing point between two equilibria, the steady-state solution is uniquely determined. Moreover, the stability of the solution is related to that of the involved equilibria.

We find that both the wave types and the stability of the steady-state solution depend on the total number N of vehicles on the ring road, and that the simulation results agree with the analysis in general. For the case with a realistic relaxation time $\tau = 0.3s$, a casually distributed traffic state (of Eq. (30)) is able to stably evolve into the corresponding steady-state flow for light or heavy traffic with small or large number N , but liable to generate stop-and-go waves for congested traffic with the number N that is between. This tendency is similar to that on a homogeneous level ring road, and the indicated phenomena are physically significant for a better understanding and the management of traffic flow on an inhomogeneous road in general.

However, we still need more efficient tools for stability analysis of the discussed steady-state solution due to the inadequate lengths of and the neglect of interaction between the involved equilibrium states in the current analysis.

Acknowledgements

The study was jointly supported by grants from the National Natural Science Foundation of China (11072141, 11272199), the National Basic Research Program of China (2012CB725404), Shanghai Program for Innovative Research Team in Universities, the Research Grants Council of the Hong Kong Special Administrative Region, China (Grant No. HKU7184/10E), and a National Research Foundation of Korea grant funded by the Korean government (MEST) (NRF-2010-0029446).

References

- [1] W. Jin, and H.M. Zhang, The inhomogeneous kinematic wave traffic flow model as a resonant nonlinear system. *Transportation Science*, 37(2003), 294-311.
- [2] P. Zhang and R.X. Liu, Hyperbolic conservation laws with space-dependent flux: I Characteristics theory and Riemann problem, *J. Comput. Appl. Math.* 156(2003), 1-21.
- [3] P. Zhang, R.X. Liu and S.C. Wong, High-resolution numerical approximation of traffic flow problems with variable lanes and free flow velocities, *Phys. Rev. E*, 71(2005), 056704.
- [4] P. Zhang, S.C. Wong and Z.L. Xu, A hybrid scheme for solving a multi-class traffic flow model with complex wave breaking, *Computer Methods in Applied Mechanics Engineering*, 197(45-48)(2008), 3816-3827.
- [5] P. Zhang, D.Y. Wu, S.C. Wong and Y.Z. Tao, Kinetic description of bottleneck effects in traffic flow, *Appl. Math. Mech. -Engl. Ed.* 30(4)(2009), 425-434.
- [6] R. Bürger, A. Gracia, K.H. Karlsen, J.D. Towers, A family of numerical schemes for kinematic flows with discontinuous flux, *Journal of Engineering Mathematics*, 60(2008), 387-425.

- [7] R. Bürger, A. Gracia, K.H. Karlsen, J.D. Towers, Difference schemes, entropy solutions, and speedup impulse for an inhomogeneous kinematic traffic flow model, *Network Heterogeneous Media*, 3(2008), 1-41.
- [8] W.J. Sun, S.C. Wong, P. Zhang, C.-W. Shu, Shock-fitting algorithm for the LWR model on inhomogeneous highways. *Transportmetrica*, 7(2)(2011), 163-180.
- [9] R. Nagai, H. Hanaura, K. Tanaka and T. Nagatani, Discontinuity at edge of traffic jam induced by slowdown, *Physica A*, 364(2006), 464-472.
- [10] K. Tanaka, H. Hanaura and T. Nagatani, Traffic jam and discontinuity induced by slowdown in two-stage optimal-velocity model, *Physica A*, 370(2006), 756-768.
- [11] H. Hanaura, T. Nagatani and K. Tanaka, Jam formation in traffic flow on a highway with some slowdown sections, *Physica A*, 374(2007), 419-430.
- [12] J. Ward, R.E. Wilson and P. Berg, Multiscale analysis of a spatially heterogeneous microscopic traffic model, *Physica D*, 236(2007), 1-12.
- [13] X.L. Li, T. Song, H. Kuang, and S.Q. Dai, Phase transition on speed limit traffic with slope, *Chinese Physics B*, 17(8)(2008), 3014-3020.
- [14] H.D. He, W.Z. Lu, Y. Xue and L.Y. Dong, Dynamic characteristics and simulation of traffic flow with slope, *Chinese Physics B*, 18(7)(2009), 2703-2708.
- [15] M.J. Lighthill and G.B. Whitham, On kinematic waves: II. A theory of traffic flow on long crowded roads, *Proc. Roy. Soc. London, Ser. A*, 22(1955), 317-345.
- [16] P.I. Richards, Shockwaves on the highway, *Operations Research*, 4(1956), 42-51.
- [17] P. Zhang, C.X. Wu and S.C. Wong, A semi-discrete model and its approach to a solution for wide moving jam in traffic flow, *Physica A* 391(3) (2012), 456-463.
- [18] B. S. Kerner and P. Konhauser, Structure and parameters of clusters in traffic flow, *Phys. Rev. E*, 50(1994), 54-83.
- [19] P. Zhang and S.C. Wong, Essence of conservation forms in the traveling wave solutions of Higher-Order Traffic Flow Model, *Phys. Rev. E* 74(2006), 026109.
- [20] R.Y. Xu, P. Zhang, S.Q. Dai and S.C. Wong, Admissibility of a wide cluster solution in “anisotropic” higher-order traffic flow models, *SIAM J. Appl. Math.* 68(2007), 562-573.
- [21] W.L. Jin, H.M. Zhang, The formation and structure of vehicle clusters in the Payne-Whitham traffic flow model, *Transp. Res. Part B* 37(2003) 207-223.
- [22] B.S. Kerner, *The Physics of Traffic*, Springer, Berlin, New York, (2004).
- [23] B.S. Kerner, Complexity of spatiotemporal traffic phenomena in flow of identical drivers: Explanation based on fundamental hypothesis of three-phase theory, *Phys. Rev. E* 85(2012), 036110.
- [24] B.S. Kerner et al., Traffic dynamics in empirical probe vehicle data studied with three-phase theory: Spatiotemporal reconstruction of traffic phases and generation of jam warning messages, *Physica A* 392(2013), 221-251.
- [25] T. Seidel, I. Gasser, and B. Werner, Microscopic Car-Following Models Revisited: From Road Works to Fundamental Diagrams, *SIAM J. Applied Dynamical Systems* 8(3)(2009), 1305-1323.
- [26] I. Gasser, and B. Werner, Dynamical phenomena induced by bottleneck, *Phil. Trans. R. Soc. A* 368(2010), 4543-4562.
- [27] J. Greenberg, Extensions and amplifications of a traffic model of Aw and Rascle, *SIAM J. Appl. Math.*, 62(2001), 729-745.
- [28] J.M. Greenberg, Congestion redux, *SIAM J. Appl. Math.*, 64(4)(2004), 1175-1185.
- [29] A. Aw, A. Klar, T. Materne, and M. Rascle, Derivation of continuum traffic flow models from microscopic follow-the-leader models, *SIAM J. Appl. Math.*, 63(2002), 259-278.
- [30] A. Aw and M. Rascle, Resurrection of “second order” models of traffic flow, *SIAM J. Appl. Math.*, 60(2000), 916-938.
- [31] M. Rascle, An improved macroscopic model of traffic flow: Derivation and links with the Lighthill-Whitham model, *Math. Comput. Modelling*, 35(2002), 581-590.

- [32] H.M. Zhang, A non-equilibrium traffic model devoid of gas-like behavior, *Transp. Res. Part B*, 36 (2002), 275-290.
- [33] H.M. Zhang, Comment on “On the controversy around Daganzo’s requiem for and Aw-Rascle’s resurrection of second- order traffic flow models” by D. Helbing and A.F. Johansson, *Eur. Phys. J. B*, 69(2009), 563-568.
- [34] R.G. Zhou, L.S. Jiang and J. F. Sun, The study of highway gradient and grade length limit, *Journal of Highway and Transportation Research and Development*, 21(7), (2004).
- [35] M. Bando, K. Hasebe, A. Nakayama, A. Shibata and Y. Sugiyama, Dynamical model of traffic congestion and numerical simulation, *Phys. Rev. E*, 51(1995), 1035-1042.
- [36] S. Jin and Z.P. Xin, Numerical passage from systems of conservation laws to Hamilton-Jacobi equations, and relaxation schemes. *SIAM J. Numer. Anal.*, 35(6)(1998), 2385-2404.
- [37] S. Jin, L. Pareschi and G. Toscani. Uniformly accurate diffusive relaxation schemes for multiscale transport equations. *SIAM J. Numer. Anal.*, 38(3)(2000), 913-936.
- [38] M. Herty, L. Pareschi and M. Seaid. Discrete-velocity models and relaxation schemes for traffic flows. *SIAM Journal on Scientific Computing*, 28(2006), 1582-1596.
- [39] Sugiyama Y et al., Traffic jams without bottlenecks-experimental evidence for the physical mechanism of the formation of a jam. *New Journal of Physics*, 10(2008), 033001.